



Comparison of selenate and selenite adsorption from aqueous solutions on the mesoporous goethite: kinetics, equilibrium and mechanism

Shifeng Li^{a,b,*}, Feng Lu^b, Shuhua Yao^{b,*}, Shuyan Zang^b

^aKey Laboratory of Pollution Ecology and Environmental Engineering, Institute of Applied Ecology, Chinese Academy of Sciences, Shenyang 110016, China, email: li.shi.feng@163.com

^bLiaoning Engineering Research Center for Treatment and Recycling of Industrially Discharged Heavy Metals, Shenyang University of Chemical Technology, Shenyang 110142, China, emails: Ysh1997@163.com (S.H. Yao), 1134605379@qq.com (F. Lu), zangshuyan@126.com (S.Y. Zang)

Received 16 July 2020; Accepted 13 December 2020

ABSTRACT

The mesoporous goethite synthesized by the hydrothermal method was employed to remove selenate (Se(VI)) and selenite (Se(IV)) from wastewater. The adsorption data of kinetics and isotherms were determined and fitted with different models, and the potential adsorption mechanism was discussed according to X-ray photoelectron spectroscopy (XPS) analysis. The maximum adsorption capacities of Se(IV) and Se(VI) on the mesoporous goethite are 71.07 and 21.07 mg/g at 25°C, respectively, which are about two orders of magnitude higher than the natural goethite. The XPS results revealed that the Se(IV) was adsorbed on the surface of the mesoporous by the formation of the inner-sphere complex, but the outer-sphere complexes are formed with Se(VI). The mesoporous goethite is expected to be a potential adsorbent for Se removal from industrial selenium-containing wastewater on a large scale for its properties of easy-preparation and less cost compared with classic nanomaterials.

Keywords: Mesoporous goethite; Selenite; Selenate; Adsorption; Surface complexation

1. Introduction

Selenium is an essential trace element and plays a key role in the health of the human body at low levels [1]. However, selenium pollution has become an increasingly severe environmental problem due to the extended-release of Se-containing wastewater into the natural environment derived from anthropogenic activity [2]. Selenium mainly exists in four oxidation states (-II, 0, IV, VI). As high bio-availability and potential toxicity, selenate (Se(VI)) and selenite (Se(IV)) have attracted increasing attention in wastewater treatment [2]. It has been noted that adsorption technology has been documented as the prior way to remove heavy metals wastewater due to its highly efficient and regenerative nature [2–9]. For instance, carbon materials

with a high specific surface area such as carbon nanotubes, activated carbon have shown excellent applications for Se removal [10,11]. Meanwhile, several recent studies have documented that Se(IV) can be readily adsorbed on metal oxides by the formation of surface complexes [12–15]. However, for the removal of Se(VI), the adsorption process has failed to reach a satisfactory result [11–17]. Despite recent advances in the Se(VI) and Se(IV) adsorption behaviors, kinetics, thermodynamics on the mentioned-above sorbents, there remain numerous challenges that limit their practical use, such as the high-cost and the preparation complexity of sorbents [18–20]. Recent studies have demonstrated that iron oxides or oxy-hydroxides were especially useful adsorbents in the field of pollution

* Corresponding authors.

removal as their strong affinity for anion species [11–17,21–26]. More importantly, they are widely distributed in nature and can be synthesized readily on a large scale. For example, goethite is the most stable iron oxyhydroxide in the natural environment and has excellent surface activity. So, natural goethite or synthetic goethite have been extensively employed to remove heavy metals such as As(V), Se(IV), and Se(VI) from wastewater [15,16,21,23]. However, the comparison of adsorption characteristics of Se(IV) and Se(VI) onto goethite and the adsorption mechanism seems to remain poorly understood [3,27].

In this work, the mesoporous goethite was applied to remove Se(IV) and Se(VI) from water, and the adsorption kinetics, isotherms, thermodynamic analysis, and mechanism were investigated. This study aimed to provide a simple and low-cost method for mesoporous goethite synthesis and to compare the adsorption performance and mechanism of Se(VI) and Se(IV) on the mesoporous goethite. The research results are expected to provide some useful information in the future for industrial selenium-containing wastewater treatment on a large scale.

2. Experimental

2.1. Materials

$\text{FeSO}_4 \cdot 7\text{H}_2\text{O}$, H_2O_2 (30%), KBH_4 , NaOH , and HCl were obtained from Aladdin Reagent (China). Na_2SeO_4 and Na_2SO_3 were purchased from Sinopharm Chemical Reagent Co., Ltd., (China). Selenium stock solutions (500 mg/L) were prepared by dissolving Na_2SeO_4 and Na_2SO_3 into ultrapure water, respectively. The mesoporous goethite was synthesized by the oxidation of ferrous sulfate heptahydrate with hydrogen peroxide following the method reported by Xiao et al. [28], and the reaction equation is described as follows:



2.2. Characterization

The crystal structure of mesoporous goethite was characterized by X-ray diffraction (XRD) (Bruker D8 ADVANCE, Germany). The transmission electron microscope (TEM; Tecnai G220, USA) was used to observe the surface morphology of mesoporous goethite. The chemical species of the surface O and Fe elements on the mesoporous goethite were determined before and after Se(VI) and Se(IV) adsorption by an X-ray photoelectron spectrometer (Thermo Scientific 250Xi, USA). The Se(IV) and Se(VI) concentrations were detected with the hydride generation-atomic fluorescence spectrometry (Jinsuokun SK-2003AZ, China) [27].

2.3. Adsorption experiments

The batch adsorption experiments were carried out as a function of the mesoporous goethite dosage, initial pH value of the Se solution. The effect of the mesoporous goethite dosage on the Se(IV) or Se(VI) adsorption capacity

was studied with the Se solution concentration of 10 mg/L at ambient temperature and pH of 6.0. The effect of the initial pH value of the Se solution was investigated when the pH varied in the range of 4.0–9.0 at 25°C. The concentration of Se(IV) or Se(VI) in the filtrate was determined by a hydride generation-atomic fluorescence spectrometry.

2.4. Adsorption kinetics experiments

0.195 g mesoporous goethite was added to a beaker flask containing 750 mL Se(VI) or Se(IV) solution (initial Se concentration of 10 mg/L). The initial pH of the Se solution was adjusted to 6.0. The mixture was shaken for 5 h at ambient temperature. An aliquot of the supernatant was taken out from the suspensions at certain intervals throughout the experiment, and then the Se(IV) or Se(VI) concentration was analyzed immediately.

2.5. Isothermal adsorption experiments

In each experiment of adsorption isotherms, 0.26 g/L of mesoporous goethite was used. Se(IV) or Se(VI) solutions prepared at five concentrations (10, 50, 100, 150, and 200 mg/L) were used. The initial concentration from 10 to 200 mg/L was prepared, and the pH of the Se solution was pre-adjusted to 7.0 before adsorption tests. The adsorption isotherms of Se(VI) or Se(IV) on the mesoporous goethite at different temperatures (25°C, 35°C, and 45°C) were investigated. After the adsorption equilibrium was reached, the suspensions were taken out, filtered immediately, and analyzed.

3. Results and discussion

3.1. Characterization

Fig. 1 shows the XRD patterns of prepared mesoporous goethite. The peaks appearing in Fig. 1 can be well indexed to orthorhombic $\alpha\text{-FeOOH}$ (JCPDS No. 29-0713) [28].

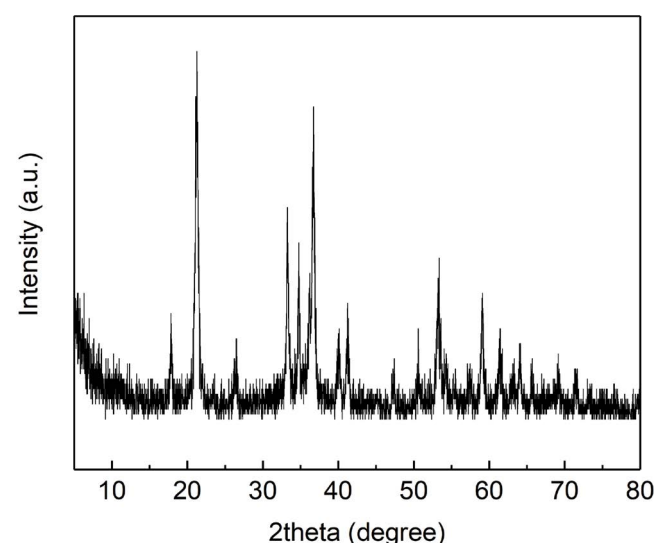


Fig. 1. XRD patterns of the mesoporous goethite.

The transmission electron microscope image of mesoporous goethite (Fig. 2) showed the typical morphology composing of dispersed rod-like particles with roughly 5 nm in diameters and about 30 nm in length.

3.2. Effect of dosage

Fig. 3 illustrates the effect of adsorbent dosage on Se(VI) and Se(IV) removal rates at the initial Se solution

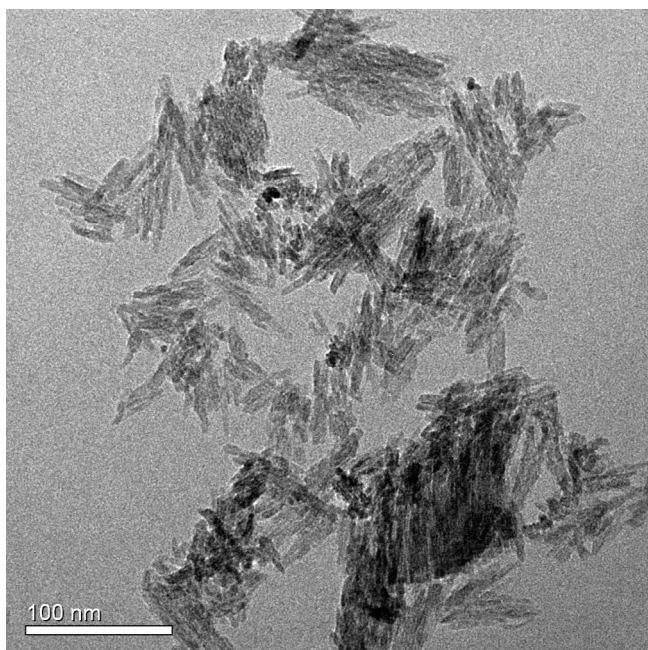


Fig. 2. Transmission electron micrograph of the mesoporous goethite.

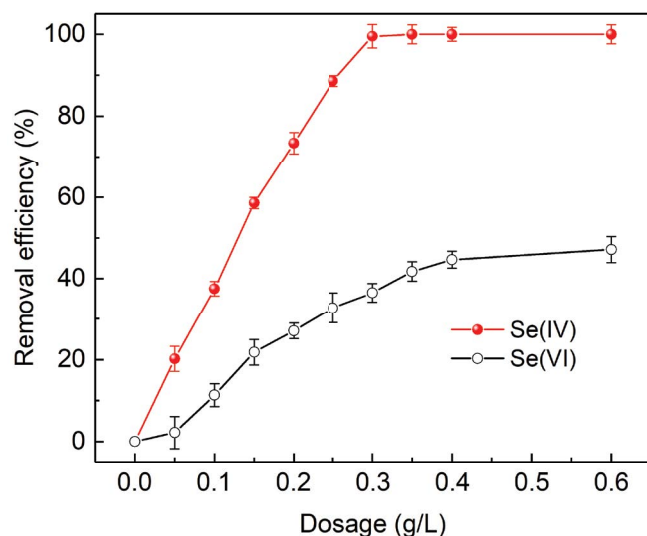


Fig. 3. Effect of adsorbent dosage on the Se(VI) or Se(IV) removal rate. (Initial Se(IV)/(VI) concentration: 10 mg/L; initial pH: 6.0; T: 25°C).

pH 6.0. The removal rate rose obviously with the increase of the adsorbent dosage. And the removal rates of Se(IV) were much higher than Se(VI) under the same goethite dosage. The difference in removal rate can be explained based on the higher relative affinity of mesoporous goethite surface sites for Se(IV) compared to Se(VI) [16–18]. More details on the Se(VI) and Se(IV) adsorption capacity on the mesoporous goethite are discussed in the subsequent adsorption isotherms section. For comparison, the same adsorbent dosage (0.26 g/L) has been employed in all the following cases.

3.3. Effect of initial pH

The effects of the initial pH on the Se removal rate on the mesoporous goethite is shown in Fig. 4. When the pH varied from 4.0 to 9.0, the removal rates of Se(IV) and Se(VI) were gradually decreased with the increasing of pH, which is similar to the trends for anions adsorption on the metal oxides (or oxy-hydroxides) [16,17]. Many studies have explored that the speciation of Se(VI) and Se(IV) under different pH has a significant impact on Se removal rate. As we know, Se(VI) generally exists as SeO_4^{2-} , whereas HSeO_3^- is the primary species Se(IV) at neutral conditions [2]. So, it may be associated with the increase in positive surface charge with the decrease of pH [21].

3.4. Adsorption kinetics

Fig. 5 shows the Se(VI) and Se(IV) adsorption kinetics curves on the mesoporous goethite, respectively. The adsorption capacities of Se(VI) and Se(IV) increased with the increase of contact time. Furthermore, Fig. 5 presents the adsorption capacity of Se(IV) was much higher than that of Se(VI). This finding is in accordance with the present results.

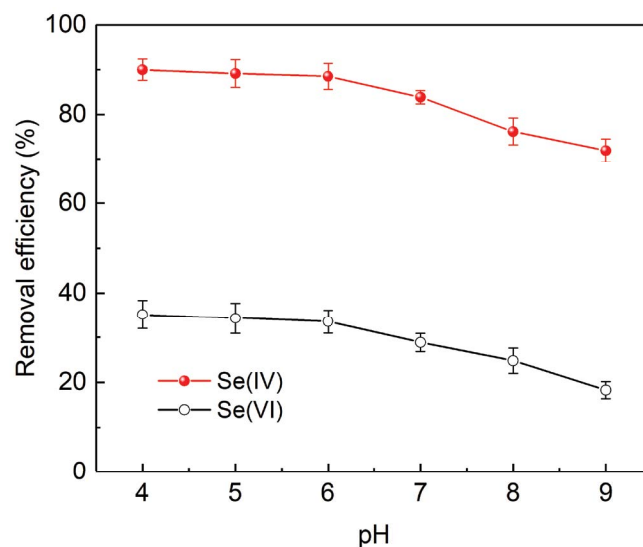


Fig. 4. Effect of initial pH on the Se(VI) or Se(IV) removal rate. (Initial Se(IV)/(VI) concentration: 10 mg/L; adsorbent dose: 0.26 g/L; T: 25°C).

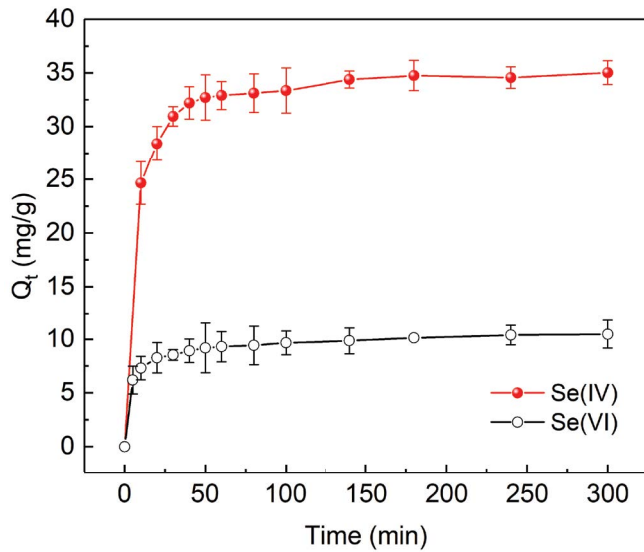


Fig. 5. Se(IV) and Se(VI) adsorption kinetics by the mesoporous goethite. (Initial Se(IV)/(VI) concentration: 10 mg/L; adsorbent dose: 0.26 g/L; initial pH: 6.0; T : 25°C).

The adsorption kinetics data were fitted by the pseudo-first-order and the pseudo-second-order kinetic models [1,29–33]. Fig. 6 shows the linear regressions of kinetics data. The kinetics process can be evaluated by the kinetic parameters such as rate constant (k) and correlation coefficients (R^2), and the results are listed in Table 1. It can be seen from data in Table 1 that the R^2 of the pseudo-second-order model (>0.999) are higher than those of the pseudo-first-order model ($R^2 = 0.8369–0.9489$), which indicated that the adsorption kinetics data could be described well by the pseudo-second-order model. Moreover, the theoretical equilibrium adsorption capacity ($Q_{e,cal}$) calculated by the pseudo-second-order model coincides with the experimental data ($Q_{e,exp}$). The model-fitting results indicated that the adsorption processes of Se(IV) and Se(VI) on the mesoporous goethite were controlled by chemical process [18].

Due to the mesoporous structure of the mesoporous goethite, diffusion is also considered to influence the adsorption kinetics. The Elovich and the intraparticle diffusion kinetic models were also employed to describe the kinetics data [34–36]. As presented in Figs. 6c and d and Table 1, the R^2 of the Elovich model ($R^2 = 0.85$ to 0.97) is lower than that of the intraparticle diffusion kinetic models ($0.91–0.98$). Notably, as shown in Fig. 6d, the first linear portion with the higher slope is assigned to film diffusion and, and the second stage is attributed to surface diffusion, which presents that the intraparticle diffusion to the sorbent surface is the rate-limiting step during the Se(VI) and Se(IV) adsorption process.

3.5. Adsorption isotherms

The adsorption isotherms at different temperatures were determined to compare the adsorption capacity of

Table 1
Kinetics model fitting parameters for Se(VI) and Se(IV) adsorption on mesoporous goethite

Kinetics models and parameters	Adsorbate	
	Se(VI)	Se(IV)
$Q_{e,exp}$	10.46	35.02
Pseudo-first-order		
k_1 (1/min)	0.0330	0.0323
$Q_{e,cal}$ (mg/g)	15.34	68.74
R^2	0.9489	0.8369
Pseudo-second-order		
k_2 (g/(mg min))	0.0130	0.0060
$Q_{e,cal}$ (mg/g)	10.61	35.46
R^2	0.9993	0.9999
Elovich		
a	5.06	20.78
b	0.99	2.72
R^2	0.9686	0.8419
Intraparticle diffusion		
k_{p1}	5.07	17.26
C_1 (mg/g)	0.64	2.43
R^2	0.9191	0.9784
k_{p2}	8.30	31.12
C_2 (mg/g)	0.13	0.24
R^2	0.9837	0.9089

Se(IV) and Se(VI) on the mesoporous goethite (Figs. 7a and 8a). And the Langmuir, Freundlich and Temkin models were employed to analyze the isotherm data, respectively [37–42]. The linear plots of the Langmuir, Freundlich, and Temkin are shown in Figs. 7b–d and 8b–d. The calculated parameters models are listed in Table 2. Table 2 shows the correlation coefficients of the Langmuir model ($R^2 > 0.993$) are higher than those of the Freundlich model ($R^2 = 0.9518–0.9806$) and the Temkin model ($R^2 = 0.9282–0.9857$), which presented that the thermodynamic adsorption data were fitted well into the Langmuir model and the adsorption process were monolayer [18]. Moreover, the maximum adsorption capacities of Se(IV) were 24–32 times higher than those of Se(VI). The findings are consistent with that of Sun et al. [18] who believed that the affinity of iron oxy-hydroxides with Se(IV) was much higher than Se(VI). The results may be explained by the fact that iron oxy-hydroxides form inner-sphere complexes with Se(IV), while the outer-sphere complexes are formed with Se(VI).

The comparisons of the maximum adsorption capacity of Se(VI) and Se(IV) between the mesoporous goethite and other Fe-based sorbents are summarized and listed in Table 3. Table 3 shows the mesoporous goethite exhibits excellent adsorption capacities of Se(IV) and Se(VI)

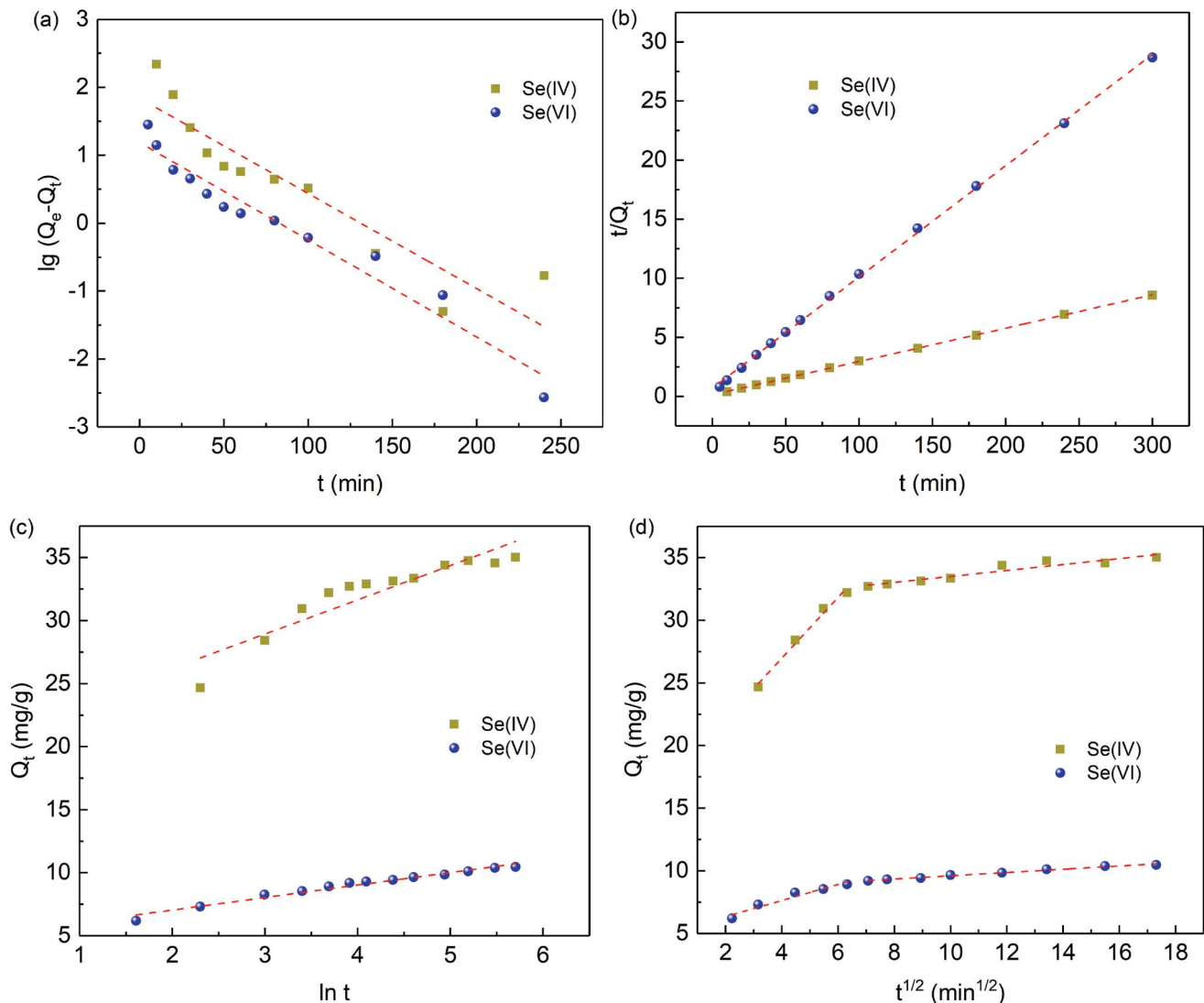


Fig. 6. (a) Pseudo-first model, (b) pseudo-second model, (c) Elovich model, and (d) intraparticle diffusion model plots of Se(VI) and Se(IV) adsorption on the mesoporous goethite.

than most of the Fe-based adsorbents reported in the literature. Notably, the adsorption capacities of Se(IV) and Se(VI) on the mesoporous goethite are about two orders of magnitude higher than the natural goethite or natural hematite, and 3–10 times as high as other Fe-based sorbents.

Meanwhile, the changes of thermodynamic parameters, such as Gibbs free energy (ΔG), enthalpy (ΔH), and entropy (ΔS) of the Se(VI) and Se(IV) adsorption on the mesoporous goethite can be obtained by the following equations [18,31,46,47]:

$$\Delta G = -RT \ln K \quad (3)$$

$$\ln K = \frac{\Delta S}{R} - \frac{\Delta H}{RT} \quad (4)$$

where the solid–liquid distribution coefficient K (L/g) can be calculated by plotting $\ln(C_e/Q_e)$ vs. C_e . The enthalpy

change (ΔH) and the entropy change (ΔS) can be calculated from Eq. (2). The results are shown in Fig. 9 and listed in Table 3. Table 4 shows the calculated enthalpy change (ΔH) and the entropy change (ΔS) during the Se(VI) adsorption on the mesoporous goethite at 298.15–308.15 K are 38.16 kJ/mol and 201.85 J/(mol K). Furthermore, the adsorption enthalpy change of Se(VI) is higher than those of Se(IV). The positive values of ΔH suggest that the Se(VI) and Se(IV) adsorption processes are endothermic, and the positive values of ΔS reflect the randomness of the solid–liquid interface between the mesoporous goethite and the Se solution. The negative Gibbs free energy (ΔG) indicates that the adsorption of Se(VI) or Se(IV) on the mesoporous goethite is a spontaneous process. Moreover, the ΔG decreases with the increase of the temperature from 298.15 to 308.15 K, suggesting that adsorption of Se(IV) or Se(VI) on the mesoporous goethite is unfavorable at high temperature [18].

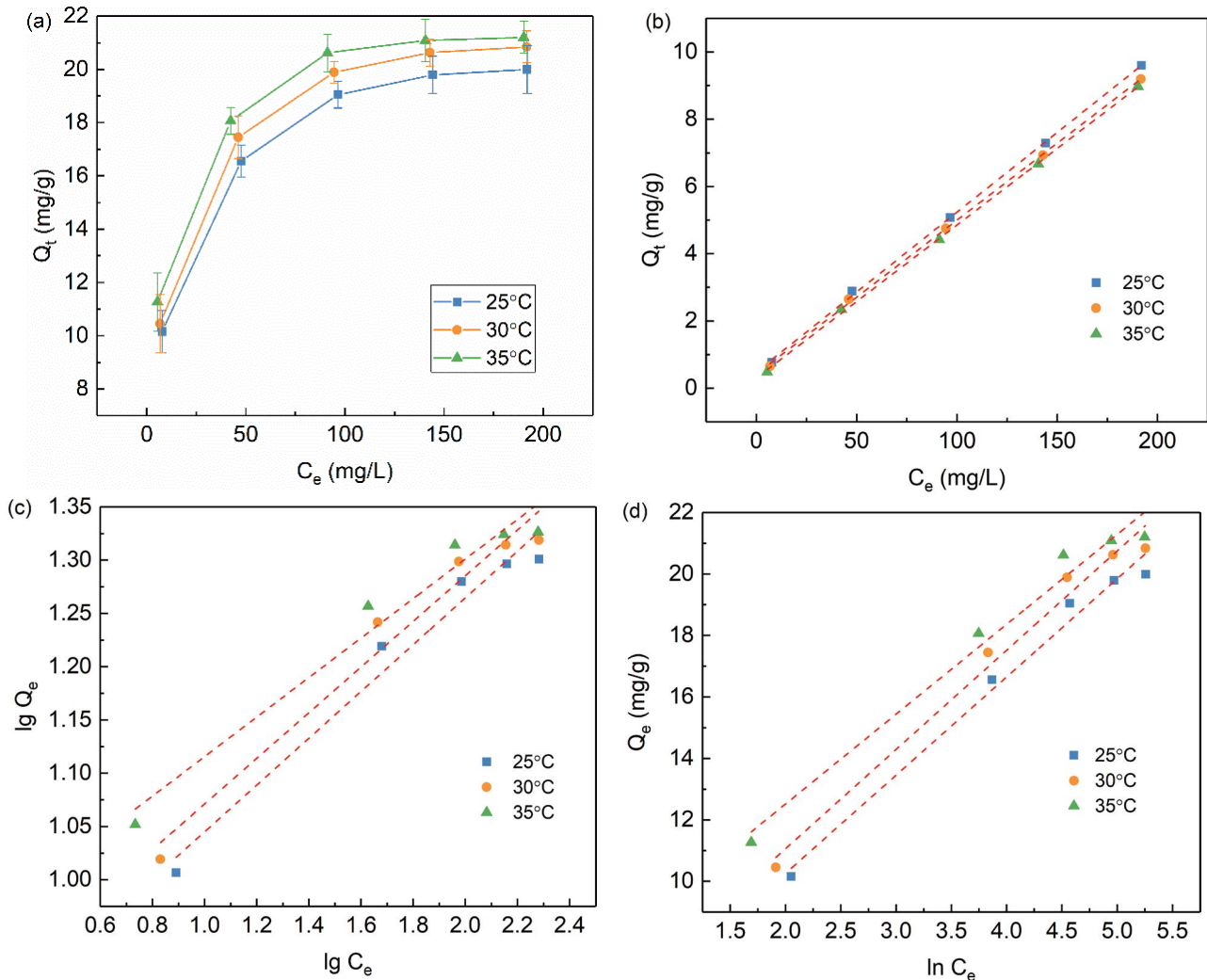


Fig. 7. Se(VI) adsorption isotherms (a) Langmuir model, (b) Freundlich model, (c) Temkin model, and (d) plots of Se(VI) adsorption on the mesoporous goethite.

3.6. Adsorption mechanism

The X-ray photoelectron spectroscopy (XPS) characterization of the mesoporous goethite before and after Se(IV) and Se(VI) adsorption was employed to clarify the potential adsorption mechanism. The high-resolution scans of Fe 2p, and O 1s for the mesoporous goethite before and after Se(VI) and Se(IV) adsorption were shown in Fig. 10. It can be seen that there are no apparent changes in the peak positions of Fe 2p after Se(VI) or Se(IV) adsorption. In Fig. 9a, the high-resolution XPS spectrum of Fe 2p presents two peaks at approximately 711.6 and 724.0 eV, which can be assigned to Fe 2p^{3/2} and Fe 2p^{1/2} of Fe³⁺, respectively [28]. As shown in Fig. 10b, the O 1s spectra of the mesoporous goethite can be deconvoluted into three peaks at about 529.9, 531.2, and 532.0 eV, respectively. And the peak at 529.9 eV can be assigned to the lattice oxygen binding with Fe (denoted as Fe–O). The peak at 531.2 eV can be ascribed to the lattice hydroxyl groups (denoted as Fe–OH). The peak at 532.0 eV can be ascribed to the adsorbed water (denoted as H₂O) [24,28]. Fig. 10c shows the content of

Fe–OH apparently decreased from 44.1% to 39.1% and the M–O content increased from 38.0% to 43.9% after adsorption of Se(IV), which show that the hydroxyl groups on the mesoporous goethite were partially placed by Se(IV) through inner-sphere complexation [18,23]. However, after Se(VI) adsorption, the decreasing of the Fe–OH content on the mesoporous goethite was not observed, and the M–O content was nearly unchanged. Therefore, Se(VI) can be adsorbed onto the mesoporous goethite surface through electrostatic attraction, that is, outer-sphere complexation. The results indirectly support previous findings, which showed the iron oxy-hydroxides form inner-sphere complexes with Se(IV), while the outer-sphere complexes are formed with Se(IV) [23,48,49].

4. Conclusion

In the present work, the mesoporous goethite synthesized by the hydrothermal method was employed to remove Se(VI) and Se(IV) from simulated wastewater. The

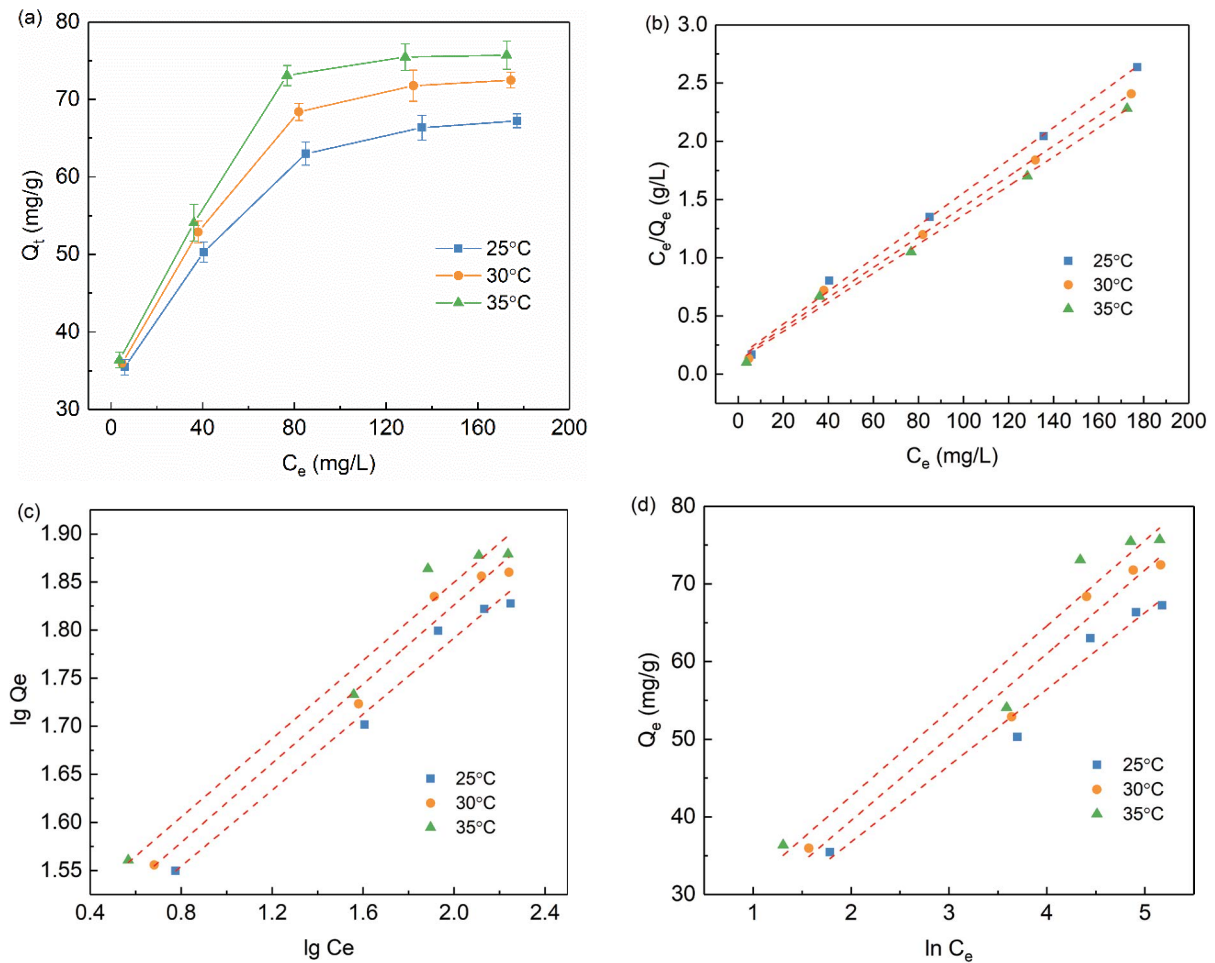


Fig. 8. Se(IV) adsorption isotherms (a) Langmuir model, (b) Freundlich model, (c) Temkin model, and (d) plots of Se(IV) adsorption on the mesoporous goethite.

Table 2
Isotherm model fitting parameters for Se(VI) and Se(IV) adsorption on mesoporous goethite

Model and parameters	Se(VI)			Se(IV)		
	Temperature (K)					
	298.15	303.15	308.15	298.15	303.15	308.15
Langmuir						
Q_{\max} (mg/g)	21.07	21.83	21.97	71.07	76.69	80.00
b (L/mg)	0.49	0.42	0.30	0.0938	0.0966	0.1072
R^2	0.9993	0.9994	0.9994	0.9959	0.9949	0.9932
Freundlich						
K_f	6.69	7.19	8.51	24.89	25.97	27.72
n	4.55	4.67	5.39	5.05	4.86	4.91
R^2	0.9599	0.9557	0.9518	0.9806	0.9753	0.9564
Temkin						
a	3.36	4.15	9.77	5.67	5.34	6.61
b	775.83	780.21	876.04	251.86	234.34	233.54
R^2	0.9857	0.9785	0.9711	0.9690	0.9584	0.9282

Table 3
Comparison of the maximum adsorption capacity of Se(VI) and Se(IV) among mesoporous goethite and other Fe-based adsorbents

Adsorbents	pH	Adsorption capacities (mg/g)		References
		Se(VI)	Se(IV)	
Natural goethite	6.0	–	8.14	[14]
Hematite	4.4	0.86	2.46	[17]
Fe ₃ O ₃ @hematite	7.0	–	25.0	[12]
Fe ₃ O ₃ -graphene oxide	6.0–9.0	15.1	23.8	[43]
α -Fe ₂ O ₃	6.0	–	17.9	[44]
CuFe ₂ O ₄	7.4 ^a	5.97	14.1	[18]
MnFe ₂ O ₄	4.0	0.77	6.57	[45]
Goethite	3.0	–	6.62	[15]
Natural goethite	4.0	0.17	0.52	[16]
Natural hematite	4.0	0.24	0.39	[16]
Mesoporous goethite	6.0	21.07	71.07	This work

^aequilibrium pH.

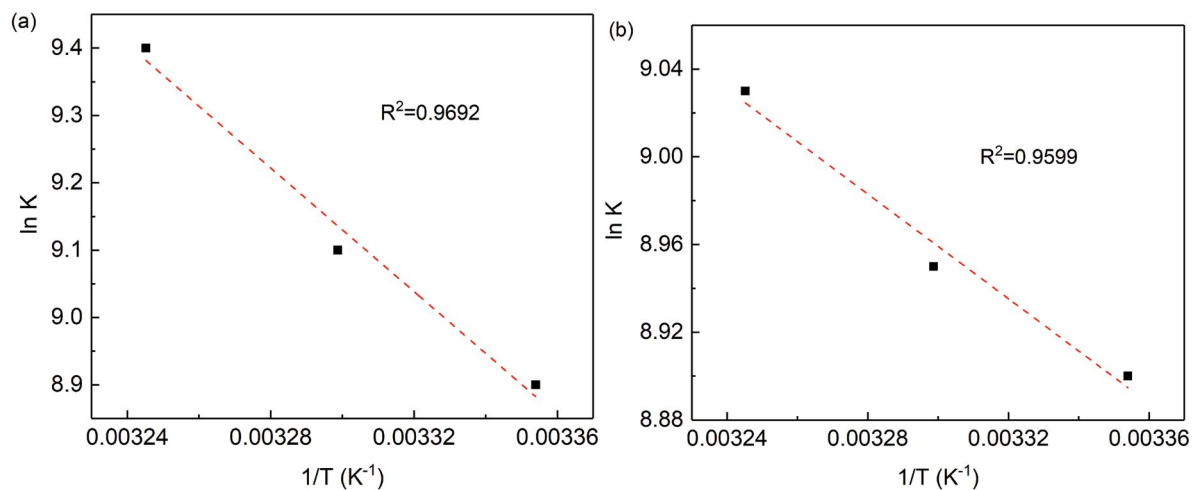


Fig. 9. Van't Hoff plots for the adsorption of (a) Se(VI) and (b) Se(IV) onto the mesoporous goethite.

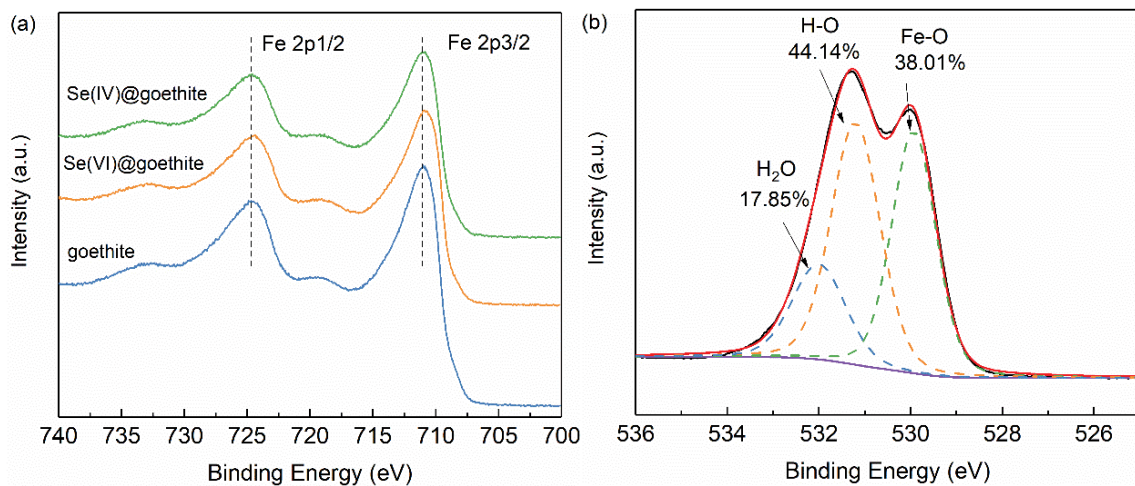


Fig. 10. XPS peaks for Fe 2p (a) and O 1s of the mesoporous goethite before (b) and after adsorption of Se(IV)

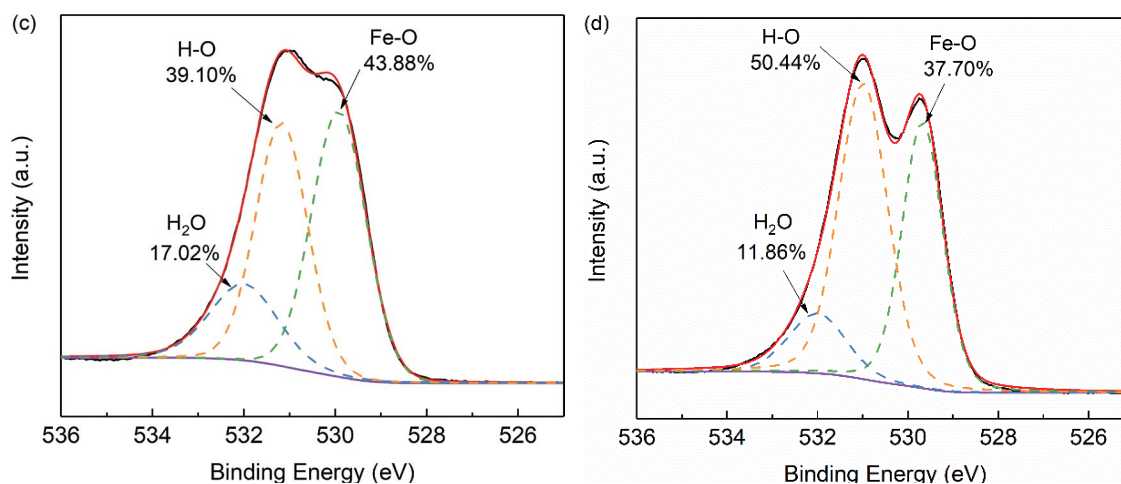


Fig. 10. XPS peaks for Fe 2p (c) and Se(VI) (d).

Table 4
Thermodynamic parameters for Se(VI) and Se(IV) adsorption on mesoporous goethite

Adsorbate	T (K)	ΔG (kJ/mol)	ΔH (kJ/mol)	ΔS (J/(mol K))
Se(VI)	298.15	-22.18	38.16	201.85
	305.15	-22.84		
	308.15	-24.04		
Se(IV)	298.15	-22.09	9.92	107.23
	305.15	-22.53		
	308.15	-23.17		

mesoporous goethite showed an excellent Se(IV) removal capacity than Se(VI). The batch experiment results show Se(IV) and Se(VI) adsorption kinetics data on the mesoporous goethite were fitted well to the pseudo-second-order model, and the maximum adsorption capacities of Se(VI) and Se(IV) on mesoporous goethite calculated by the Langmuir isotherm model were 21.07 and 71.07 mg/g at 25°C. The positive values of ΔH and the negative Gibbs free energy (ΔG) suggest that the adsorption process is endothermic and a spontaneous process. Inner-sphere complexation existed on the mesoporous goethite with Se(IV), and outer-sphere complexation may be the dominant adsorption mechanism.

Acknowledgments

We thank the Scientific Research Fund of Liaoning Provincial Education Department (No. LQ2020027), the National Key R&D Program of China (No. 2017YFD0800301), the China Postdoctoral Science Foundation (No. 2015M571343), the Scientific Research Program of the Sheyang University of Chemical Technology (No. XXL2019003), and the Shenyang High-level Innovative Talents Project (RC180011) for the financial support.

References

- [1] B. Singha, S.K. Das, Biosorption of Cr(VI) ions from aqueous solutions: kinetics, equilibrium, thermodynamics and desorption studies, *Colloids Surf., B*, 84 (2011) 221–232.

- [2] Y.Z. He, Y.J. Xiang, Y.Y. Zhou, Y. Yang, J.C. Zhang, H.L. Huang, C. Shang, L. Luo, J. Gao, L. Tang, Selenium contamination, consequences and remediation techniques in water and soils: a review, *Environ. Res.*, 164 (2018) 288–301.
- [3] J. Stefaniak, A. Dutta, B. Verbinnen, M. Shakya, E.R. Rene, Selenium removal from mining and process wastewater: a systematic review of available technologies, *J. Water Supply Res. Technol. AQUA*, 67 (2018) 903–918.
- [4] H.-T. Fan, W. Sun, B. Jiang, Q.-J. Wang, D.-W. Li, C.-C. Huang, K.-J. Wang, Z.-G. Zhang, W.-X. Li, Adsorption of antimony(III) from aqueous solution by mercapto-functionalized silica-supported organic-inorganic hybrid sorbent: mechanism insights, *Chem. Eng. J.*, 286 (2016) 128–138.
- [5] T.K. Naiya, A.K. Bhattacharya, S.K. Das, Adsorption of Cd(II) and Pb(II) from aqueous solutions on activated alumina, *J. Colloid Interface Sci.*, 333 (2009) 14–26.
- [6] T. Tatarchuk, A. Shyichuk, I. Mironyuk, Mu. Naushad, A review on removal of uranium(VI) ions using titanium dioxide based sorbents, *J. Mol. Liq.*, 293 (2019) 11563, <https://doi.org/10.1016/j.molliq.2019.111563>.
- [7] T. Tatarchuk, N. Paliychuk, R.B. Bitra, A. Shyichuk, Mu. Naushad, I. Mironyuk, D. Ziolkowska, Adsorptive removal of toxic Methylene Blue and Acid Orange 7 dyes from aqueous medium using cobalt-zinc ferrite nano-adsorbents, *Desal. Water Treat.*, 150 (2019) 374–385.
- [8] I. Mironyuk, T. Tatarchuk, Mu. Naushad, H. Vasylyeva, I. Mykytyn, Highly efficient adsorption of strontium ions by carbonated mesoporous TiO₂, *J. Mol. Liq.*, 285 (2019) 742–753.
- [9] E. Bazrafshan, M. Sobhanikia, F.K. Mostafapour, H. Kamani, D. Balarak, Chromium biosorption from aqueous environments by mucilaginous seeds of *Cydonia oblonga*: thermodynamic, equilibrium and kinetic studies, *Global NEST J.*, 19 (2017) 269–277.
- [10] R. Kamaraj, S. Vasudevan, Decontamination of selenate from aqueous solution by oxidized multi-walled carbon nanotubes, *Powder Technol.*, 274 (2015) 268–275.
- [11] G.B. Jegadeesan, K. Mondal, S.B. Lalvani, Adsorption of Se(IV) and Se(VI) using copper-impregnated activated carbon and fly ash-extracted char carbon, *Water Air Soil Pollut.*, 226 (2015), <https://doi.org/10.1007/s11270-015-2520-5>.
- [12] Z.Y. Ma, C. Shan, J.L. Liang, M.P. Tong, Efficient adsorption of selenium(IV) from water by hematite modified magnetic nanoparticles, *Chemosphere*, 193 (2018) 134–141.
- [13] S.F. Evans, M.R. Ivancevic, J.Q. Yan, A.K. Naskar, A.M. Levine, R.J. Lee, C. Tsouris, M.P. Paranthaman, Magnetic adsorbents for selective removal of selenite from contaminated water, *Sep. Sci. Technol.*, 54 (2019) 2138–2146.
- [14] A.T. Jacobson, M.H. Fan, Evaluation of natural goethite on the removal of arsenate and selenite from water, *J. Environ. Sci.*, 76 (2019) 133–141.
- [15] M. Matulová, M. Urík, M. Bujdoš, E. Duborská, M. Cesnek, M.B. Miglierini, Selenite sorption onto goethite: isotherm

- and ion-competitive studies, and effect of pH on sorption kinetics, *Chem. Pap.*, 73 (2019) 2975–2985.
- [16] M. Rovira, J. Giménez, M. Martínez, X. Martínez-Lladó, J. de Pablo, V. Martí, L. Duro, Sorption of selenium(IV) and selenium(VI) onto natural iron oxides: goethite and hematite, *J. Hazard. Mater.*, 150 (2008) 279–284.
- [17] M.J. Jang, S.Y. Pak, M.-J. Kim, Comparison of adsorption characteristics of Se(IV) and Se(VI) onto hematite: effects of reaction time, initial concentration, pH, and ionic strength, *Environ. Earth Sci.*, 74 (2015) 1169–1173.
- [18] W.L. Sun, W.Y. Pan, F. Wang, N. Xu, Removal of Se(IV) and Se(VI) by MFe_2O_4 nanoparticles from aqueous solution, *Chem. Eng. J.*, 273 (2015) 353–362.
- [19] N. Gezer, M. Gülsen, A.O. Aydın, Adsorption of selenite and selenate ions onto thiourea-formaldehyde resin, *J. Appl. Polym. Sci.*, 122 (2011) 1134–1141.
- [20] J.M. Wei, W. Zhang, W.Y. Pan, C.R. Li, W.L. Sun, Experimental and theoretical investigations on Se(IV) and Se(VI) adsorption to UiO-66-based metal-organic frameworks, *Environ. Sci.: Nano*, 5 (2018) 1441–1453.
- [21] K. Kalaizidou, A.-A. Nikolettopoulos, N. Tsiftsakis, F. Pina-kidou, M. Mitrakas, Adsorption of Se(IV) and Se(VI) species by iron oxy-hydroxides: effect of positive surface charge density, *Sci. Total Environ.*, 687 (2019) 1197–1206.
- [22] A. Onoguchi, G. Granata, D. Haraguchi, H. Hayashi, C. Tokoro, Kinetics and mechanism of selenate and selenite removal in solution by green rust-sulfate, *R. Soc. Open Sci.*, 6 (2019) 182147, doi: 10.1098/rsos.182147.
- [23] J.S. Zhang, R.S. Stanforth, S.O. Pehkonen, Effect of replacing a hydroxyl group with a methyl group on arsenic(V) species adsorption on goethite (α -FeOOH), *J. Colloid Interface Sci.*, 306 (2007) 16–21.
- [24] F. Yang, S.S. Zhang, H.P. Li, S.S. Li, K. Cheng, J.-S. Li, D.C.W. Tsang, Corn straw-derived biochar impregnated with α -FeOOH nanorods for highly effective copper removal, *Chem. Eng. J.*, 348 (2018) 191–201.
- [25] E.M. Cálix, L.C. Tan, E.R. Rene, Y.V. Nancharaiiah, E.D. Van Hullebusch, P.N.L. Lens, Simultaneous removal of sulfate and selenate from wastewater by process integration of an ion exchange column and upflow anaerobic sludge blanket bioreactor, *Sep. Sci. Technol.*, 54 (2019) 1387–1399.
- [26] S. Hasan, A. Ghosh, K. Race, R. Schreiber Jr., M. Prelas, Dispersion of FeOOH on chitosan matrix for simultaneous removal of As(III) and As(V) from drinking water, *Sep. Sci. Technol.*, 49 (2014) 2863–2877.
- [27] G.L. Zhang, M.A. Gomez, S.H. Yao, X. Ma, S.F. Li, X. Cao, S.Y. Zang, Y.F. Jia, Systematic study on the reduction efficiency of ascorbic acid and thiourea on selenate and selenite at high and trace concentrations, *Environ. Sci. Pollut. Res.*, 26 (2019) 10159–10173.
- [28] M. Xiao, Y.P. Zhao, S.F. Li, Facile synthesis of chrysanthemum-like mesoporous α -FeOOH and its adsorptive behavior of antimony from aqueous solution, *J. Dispersion Sci. Technol.*, 41 (2020) 1812–1820.
- [29] S.K. Lagergren, About the theory of so-called adsorption of soluble substances, *Kungliga Svenska Vetensk. Handl.*, 24 (1898) 1–39.
- [30] Y.S. Ho, G. McKay, A comparison of chemisorption kinetic models applied to pollutant removal on various sorbents, *Process Saf. Environ. Prot.*, 76 (1998) 332–340.
- [31] H.-T. Fan, Y. Sun, Q. Tang, W.-L. Li, T. Sun, Selective adsorption of antimony(III) from aqueous solution by ion-imprinted organic-inorganic hybrid sorbent: kinetics, isotherms and thermodynamics, *J. Taiwan Inst. Chem. Eng.*, 45 (2014) 2640–2648.
- [32] S. Vasudevan, B.S. Kannan, J. Lakshmi, S. Mohanraj, G. Sozhan, Effects of alternating and direct current in electrocoagulation process on the removal of fluoride from water, *J. Chem. Technol. Biotechnol.*, 86 (2011) 428–436.
- [33] S. Vasudevan, J. Lakshmi, G. Sozhan, Studies relating to removal of arsenate by electrochemical coagulation: optimization, kinetics, coagulant characterization, *Sep. Sci. Technol.*, 45 (2010) 1313–1325.
- [34] H.A. Taylor, N. Thon, Kinetics of chemisorption, *J. Am. Chem. Soc.*, 74 (1952) 4169–4173.
- [35] W.J. Weber, J.C. Morris, Kinetics of adsorption on carbon from solution, *J. Sanit. Eng. Div.*, 89 (1963) 31–60.
- [36] H.-T. Fan, Q. Tang, Y. Sun, Z.-G. Zhang, W.-X. Li, Selective removal of antimony(III) from aqueous solution using antimony(III)-imprinted organic-inorganic hybrid sorbents by combination of surface imprinting technique with sol-gel process, *Chem. Eng. J.*, 258 (2014) 146–156.
- [37] I. Langmuir, The adsorption of gases on plane surfaces of glass, mica and platinum, *J. Am. Chem. Soc.*, 40 (1918) 1361–1403.
- [38] H.M.F. Freundlich, Über die adsorption in lösungen, *Zeitschrift für Physikalische Chemie*, 57 (1906) 385–470.
- [39] M. Temkin, V. Pyzhev, Kinetics of ammonia synthesis on promoted iron catalysts, *Acta Physicochim. U.R.S.S.*, 12 (1940) 327–356.
- [40] I. Mironyuk, T. Tatarchuk, H. Vasylyeva, V.M. Gun'ko, I. Mykytyn, Effects of chemisorbed arsenate groups on the mesoporous titania morphology and enhanced adsorption properties towards Sr(II) cations, *J. Mol. Liq.*, 282 (2019) 587–597.
- [41] S. Vasudevan, J. Lakshmi, R. Vanathi, Electrochemical coagulation for chromium removal: process optimization, kinetics, isotherms and sludge characterization, *Clean – Soil Air Water*, 38 (2010) 9–16.
- [42] R. Kamaraj, A. Pandiarajan, R.M. Gandhi, A. Shibayama, S. Vasudevan, Eco-friendly and easily prepared graphene nanosheets for safe drinking water: removal of chlorophenoxyacetic acid herbicides, *ChemistrySelect*, 2 (2017) 342–355.
- [43] Y. Fu, J.Y. Wang, Q.X. Liu, H.B. Zeng, Water-dispersible magnetic nanoparticle-graphene oxide composites for selenium removal, *Carbon*, 77 (2014) 710–721.
- [44] A.W. Lounsbury, J.S. Yamani, C.P. Johnston, P. Lares-Casanova, J.B. Zimmerman, The role of counter ions in nano-hematite synthesis: implications for surface area and selenium adsorption capacity, *J. Hazard. Mater.*, 310 (2016) 117–124.
- [45] C.M. Gonzalez, J. Hernandez, J.G. Parsons, J.L. Gardea-Torresdey, A study of the removal of selenite and selenate from aqueous solutions using a magnetic iron/manganese oxide nanomaterial and ICP-MS, *Microchem. J.*, 96 (2010) 324–329.
- [46] S. Vasudevan, J. Lakshmi, G. Sozhan, Optimization of the process parameters for the removal of phosphate from drinking water by electrocoagulation, *Desal. Water Treat.*, 12 (2009) 407–414.
- [47] S. Vasudevan, J. Jayaraj, J. Lakshmi, G. Sozhan, Removal of iron from drinking water by electrocoagulation: adsorption and kinetics studies, *Korean J. Chem. Eng.*, 26 (2009) 1058–1064.
- [48] T. Hiemstra, R.P.J. Rietra, W.H. Van Riemsdijk, Surface complexation of selenite on goethite: MO/DFT geometry and charge distribution, *Croat. Chem. Acta*, 80 (2007) 313–324.
- [49] Y.F. Jia, Y. Zheng, J.R. Lin, G.Q. Zhang, X. Ma, X. Wang, S.F. Wang, Surface sorption site and complexation structure of Ca^{2+} at the goethite-water interface: a molecular dynamics simulation and quantitative XANES analysis, *Bull. Environ. Contam. Toxicol.*, 103 (2019) 64–68.